Journal of Sound and Vibration 329 (2010) 819–832

Contents lists available at ScienceDirect

Journal of Sound and Vibration

journal homepage: www.elsevier.com/locate/jsvi

Theoretical modeling and characteristic analysis of moving-train induced ground vibrations

H. Xia [a,b,*], Y.M. Cao [a], G. De Roeck [b]

[a] School of Civil Engineering, Beijing Jiaotong University, Beijing 100044, China
[b] Department of Civil Engineering, Catholic University of Leuven, B3001 Heverlee, Belgium

ARTICLE INFO

Article history:
Received 6 January 2009
Received in revised form
28 September 2009
Accepted 4 October 2009
Handling Editor: L.G. Tham
Available online 28 October 2009

ABSTRACT

An integrated train–track–subsoil dynamic interaction model of moving-train induced ground vibration is developed on the basis of vehicle dynamics, track dynamics and the Green's functions of subsoil. The model takes account of the vibrations of vehicle components, the quasi-static axle loads and the dynamic excitations between the wheels and track. The analyzed results from an example show that the ground vibration characteristics have a close relationship with train speed and soil properties; the dynamic responses excited by wheel–track irregularity have big influence on the high frequency components of ground vibration; with the increase of distance to the track, the ground acceleration has the tendency of decrease, and the relevance of acceleration curves and train excitation becomes less obvious; the intersections of moving load speed-lines and subsoil dispersion curves are some resonance frequencies that cause the amplification of ground vibrations; there exists a critical speed for moving train that is close to the minimum velocity of the Rayleigh's wave in the subsoil.

1. Introduction

With the rapid development of high-speed railway and urban rail transit system, the environmental vibration induced by running trains has been given more attention. The vibration propagates from the track into the subsoil, causes the ground vibration and furthermore may arouse the secondary vibration and noise of nearby structures and buildings, which seriously influences the living and working environment of the people. Therefore, it is necessary for city builders to predict and evaluate the environmental vibration at the commencement of planning and design of a rail traffic system.

The early researches on this subject adopted empirical prediction methods and received some useful results. However, these methods depend too much on experimental data and can only be applied to some special cases. Since the empirical prediction method cannot analyze the influence parameters of ground vibrations in detail, the more realistic models for ground vibration generation and propagation are required, especially in the case of considering the effects of the track structure and the layered subsoil.

Different analytical, semi-analytical or numerical methods for the analysis of train-induced vibrations have been developed in recent years. In a series of researches, Krylov [1–3] proposed an analytical prediction model for train-induced ground vibrations, in which the quasi-static force transmitted by a sleeper is derived from the deflection curve of the track modeled as a beam on an elastic foundation. In his works, the free-field vibration was analyzed in the frequency domain by the superposition of responses caused by all sleeper forces, and the wave propagation through the soil was represented by

* Corresponding author at: School of Civil Engineering, Beijing Jiaotong University, Beijing 100044, China. Tel.: +86 10 82161656; fax: +86 10 51683340.
E-mail address: hxia@bjtu.edu.cn (H. Xia).

0022-460X/$ - see front matter © 2009 Elsevier Ltd. All rights reserved.
doi:10.1016/j.jsv.2009.10.007

the Lamb's approximate solution for the Green's function of a half-space, in which only the contribution of the surface wave was considered, while other excitation mechanisms (such as parametric excitation, wheel and rail roughness, rail joints and wheel-flats) and through-soil coupling of sleepers were not taken into account.

Recently, Lombaert [4] evaluated, through a numerical prediction method, the contributions of quasi-static excitation related to the axle loads and the dynamic excitation of random track unevenness to the track and free-field responses, for the case of InterCity and high-speed trains running at a subcritical speed, respectively. The results show that the track response is dominated by the quasi-static contribution while the free-field response is dominated by the dynamic one, indicating that the Krylov's model that accounts for quasi-static excitation alone is well suited only for predicting the ground response in the immediate vicinity of the track.

Jones and Block [5] divided the vibration observed at the track during the running of a train into two components. The first component is the quasi-static deformation due to successive passage of the train axles, and the second is the dynamic response caused by the acceleration of the train masses over the combined track and wheels irregular profiles. For analysis of vibration propagation in the ground, they used a model of wave propagation from a fixed-point harmonic load on the track. The effect of the train movement was introduced as phase terms in the summation of vibration contributions from different sleeper positions. The results of this model were compared with the measured vibrations from freight trains at a particular site. For these trains moving at speeds well below the velocities of the waves transmitting in the track and ground structure, the fixed-point load model may satisfactorily represent the propagation of the vibration.

Karlström [6] investigated ground vibrations from railways by an analytical approach. The subsoil is modeled as a stratified half-space with linearly viscoelastic layers. On top of the ground is placed a rectangular embankment, supporting the rails and the sleepers. The rails are modeled as Euler–Bernoulli beams subjected to moving forces (wheel loads), and the sleepers are modeled with anisotropic Kirchhoff plates. The solution is based on the Fourier transforms in time and along the track. In the transverse direction, the vibrations in the embankment are developed in the Fourier series and the field vibrations in the half-space with the Fourier transforms.

Sheng [7,8] modeled the ground as a structure of three-dimensional viscoelastic layers lying either on a half-space or on a rigid foundation, and modeled the track as a single rail beam, a rail pad and a sleeper mass supported by a viscoelastic ballast layer. His theoretical analysis illustrates the existence of a wave in the combined track and ground system propagating along the direction of the track with a speed controlled by, but lower than, the lowest propagating wave in the layered ground structure. In soft soils, this wave speed may be lower than the speed of some traversing passenger trains, which should be taken into account in the design. Madshus and Kaynia [9] observed large amplitudes of displacement when the train was running on the track at high speed towards its critical speed of about 180 km/h at the measurement site.

Madshus and Kaynia et al. [9,10], along with their presentation of measurements, reported the development of an FEM model composed of a moving load on a railway/embankment structure, which was coupled to a layered ground model at a series of points via the Green's functions calculated using the dynamic stiffness matrix theory.

In Japan, Takemiya [11,12] proposed a 2.5-dimensional formulation of the finite-element model considering the irregular topographies of the track. In his model, the track is modeled by an Euler–Bernoulli beam resting on the ballast on the site ground, the train movement between the negative and positive infinite distances is formulated by the relative space coordinates, and the sleeper frequencies induced by the wheels rolling on the track are replaced by the driving frequencies. The solution for the three-dimensional transmission of vibration in the layered-soils is based on the Fourier transform with respect to the horizontal coordinate and the time. The coupling of the 3-D Green's function for layered-soils and the 2.5-D FEM is accomplished by track–soil dynamic interaction.

Yang [13,14] studied the transmissibility of soils for vibrations induced by trains moving at different speeds, by establishing a 2.5-D finite/infinite element approach, where the train was simulated by a sequence of moving wheel loads that may vibrate with certain frequency. Two train speeds were considered, one is smaller and the other is greater than the Rayleigh's wave speed of the layered soils, to represent the effects of speed in the subcritical and super-critical ranges. Parametric studies were conducted, including the shear wave speed, damping ratio and stratum depth of the supporting soils, and the moving speed and vibration frequency of the traveling trains, to evaluate the effect of each parameter on the ground response induced by moving trains.

Katou [15] adopted a 3-D viscoelastic staggered-grid finite difference method (FDM) with a fourth-order accuracy in space to study the mechanism of ground vibrations induced by a high-speed train, in which the input to numerical simulations for a single wheel was a source function developed by the time-series data of forces observed from the wheels of a running Shinkansen train.

Numerical procedures for the analysis of railway-induced ground vibrations have also been presented by several authors, based on the combination of boundary element method (BEM) and finite element method (FEM). Auersch [16] presented a rather comprehensive model to calculate the dynamic compliance, using a combined FEM/BEM model for soil and track and a multi-DOF model for the vehicle. Sheng et al. [17] also used a FEM/BEM approach for the analysis of ground vibration produced by trains. These papers are based on the idea that the ground and structures such as tunnels and tracks are homogeneous in the track direction. This assumption, which simplifies the analysis to a large extent, is realistic for the study of free field motion and vehicle vibrations in many research fields. Recently, Galvín and Domínguez [18,19] presented a general and fully three-dimensional model for analysis of the soil motion and the effects of HST (high-speed train) passage on nearby surface and underground structures, by which they studied the ground vibrations in zones with local

discontinuities in the soil properties or the effects on structures such as underpasses, buildings and auxiliary structures around the track.

The literature review shows that the present-day models use some simplifications to predict the ground-borne vibrations due to railway traffic. Most assumptions are introduced for the computation of the track–soil interaction forces. Some models consider these forces to be point loadings proportional to the deflection curve of a rail on an elastic foundation. Other models assume a frequency independent stress distribution beneath the sleeper for which the time history is derived from a train–track model with the sleeper support modeled as rigid or as spring–damper systems. The soil models in literature vary from approximate solutions including only the surface wave contribution, to horizontally layered viscoelastic half-spaces. For the problems of rail traffic induced ground vibrations, wave propagation in the soil plays a crucial role as it couples the source (the track) and the receiver (ground or building). The models aim to predict traffic-induced vibration and should therefore account for the dynamic soil-structure interaction at the source and the receiver, and incorporate a model that accurately describes wave propagation in the soil. In the present work, an integrated train–track–subsoil dynamic interaction model of moving-train induced ground vibration is developed based on vehicle dynamics, track dynamics and the Green's functions of subsoil, in which are taken into account the influence of track structure and wave motion in the three-dimensional layered-soil on ground vibrations. By means of this model, the ground vibration characteristics are analyzed through an example.

2. Establishment of train–track–subsoil model

The train–track–subsoil dynamic interaction model consists of a train submodel, a track submodel and a subsoil submodel, which are linked by the vehicle–track coupling relation and the track–soil coupling relation.

2.1. Train modeling

The train model is composed of several vehicles, with each one modeled as a multiple-degrees-of-freedom vibration system consisting of one car-body, two bogies, four wheelsets, and two groups of spring–damper suspension devices. Take the ith vehicle shown in Fig. 1 as an example, two degrees-of-freedom (floating and pitching) are considered for each car-body (i.e. Z_{ci} and φ_{ci}) and each bogie (i.e. Z_{tij} and φ_{tij}), while only one degree-of-freedom for each wheelset (i.e.z_{wil}), respectively.

Since the train vibrates in small amplitude, and the wheelset and rail are linked with linear spring shown in Fig. 1, the stiffness matrix in the train model is amplitude-independent.

On the basis of vehicle dynamics, the dynamic equilibrium equation of the ith vehicle can be written as

$$\mathbf{M}_i\ddot{\mathbf{Z}}_i + \mathbf{C}_i\dot{\mathbf{Z}}_i + \mathbf{K}_i\mathbf{Z}_i = \mathbf{P}_i(t) \tag{1}$$

where $\mathbf{Z}_i$, $\dot{\mathbf{Z}}_i$ and $\ddot{\mathbf{Z}}_i$ represent respectively the displacement, velocity and acceleration vectors;

$$\mathbf{P}_i(t) = \{0\ 0\ 0\ 0\ 0\ 0\ \ -P_{i1}^{w/r}(t)\ \ -P_{i2}^{w/r}(t)\ \ \ldots\ \ -P_{iN_{wi}}^{w/r}(t)\}^T$$

is the excitation vector acting on the ith vehicle, in which $P_{il}^{w/r}(t)$ denotes the interaction force between the rail and the lth wheelset of the ith vehicle ($l = 1, 2, \ldots, N_{wi}$), mainly induced by rail irregularity; $\mathbf{M}_i$, $\mathbf{K}_i$ and $\mathbf{C}_i$ are respectively the mass,

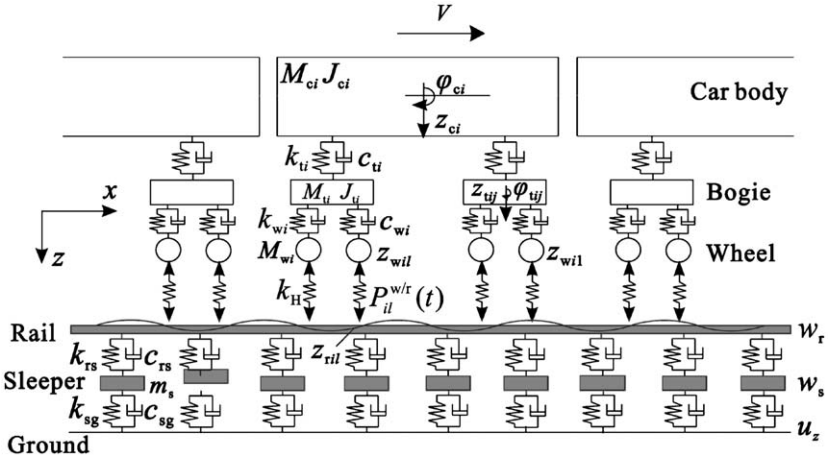

Fig. 1. Train–track dynamic interaction model.

stiffness and damping matrices of the ith vehicle, and their expansion equations are as follows:

$$\mathbf{M}_i = \mathrm{diag}[\,M_{ci} \quad J_{ci} \quad M_{ti} \quad J_{ti} \quad M_{ti} \quad J_{ti} \quad M_{wi} \quad M_{wi} \quad M_{wi} \quad M_{wi}\,] \tag{2}$$

$$\mathbf{K}_i = \begin{bmatrix} 2k_{ti} & & & & & & & & & \\ 0 & 2k_{ti}b^2 & & & \multicolumn{5}{c}{\multirow{-2}{*}{\textit{Symmetrical}}} \\ -k_{ti} & -k_{ti}b & k_{ti}+2k_{wi} & & & & & & & \\ 0 & 0 & 0 & 2k_{wi}a^2 & & & & & & \\ -k_{ti} & k_{ti}b & 0 & 0 & k_{ti}+2k_{wi} & & & & & \\ 0 & 0 & 0 & 0 & 0 & 2k_{wi}a^2 & & & & \\ 0 & 0 & -k_{wi} & -k_{wi}a & 0 & 0 & k_{wi} & & & \\ 0 & 0 & -k_{wi} & k_{wi}a & 0 & 0 & 0 & k_{wi} & & \\ 0 & 0 & 0 & 0 & -k_{wi} & -k_{wi}a & 0 & 0 & k_{wi} & \\ 0 & 0 & 0 & 0 & -k_{wi} & k_{wi}a & 0 & 0 & 0 & k_{wi} \end{bmatrix} \tag{3}$$

$$\mathbf{C}_i = \begin{bmatrix} 2c_{ti} & & & & & & & & & \\ 0 & 2c_{ti}b^2 & & & \multicolumn{5}{c}{\multirow{-2}{*}{\textit{Symmetrical}}} \\ -c_{ti} & -c_{ti}b & c_{ti}+2c_{wi} & & & & & & & \\ 0 & 0 & 0 & 2c_{wi}a^2 & & & & & & \\ -c_{ti} & c_{ti}b & 0 & 0 & c_{ti}+2c_{wi} & & & & & \\ 0 & 0 & 0 & 0 & 0 & 2c_{wi}a^2 & & & & \\ 0 & 0 & -c_{wi} & -c_{wi}a & 0 & 0 & c_{wi} & & & \\ 0 & 0 & -c_{wi} & c_{wi}a & 0 & 0 & 0 & c_{wi} & & \\ 0 & 0 & 0 & 0 & -c_{wi} & -c_{wi}a & 0 & 0 & c_{wi} & \\ 0 & 0 & 0 & 0 & -c_{wi} & c_{wi}a & 0 & 0 & 0 & c_{wi} \end{bmatrix} \tag{4}$$

in which the subscripts c, t and w denote the car-body, bogie and wheelset; M and J represent mass and pitching inertia; k and c represent the sprung stiffness coefficient and sprung damping coefficient; and a and b represent half of axle spacing and half of distance between bogies of a vehicle, respectively.

Since the matrices $\mathbf{M}$, $\mathbf{K}$ and $\mathbf{C}$ are frequency independent, the analysis is much more convenient in the frequency-domain than in the time-domain. For this, Eq. (1) is transformed from the time domain to the frequency domain by means of the Fourier transform as

$$(-\mathbf{M}_i\omega^2 + \mathrm{i}\mathbf{C}_i\omega + \mathbf{K}_i)\overline{\mathbf{Z}}_i(\omega) = \overline{\mathbf{P}}_i(\omega) \tag{5}$$

For a railway vehicle, the load vector $\overline{\mathbf{P}}_i(\omega)$ can be expressed as

$$\overline{\mathbf{P}}_i(\omega) = -\mathbf{D}\overline{\mathbf{P}}_i^{\mathrm{w/r}}(\omega) \tag{6}$$

where

$$\mathbf{D} = \begin{bmatrix} \mathbf{0}_{6\times4} \\ \mathbf{I}_{4\times4} \end{bmatrix}$$

is the factor matrix of the load vector for a four-axle vehicle, and

$$\mathbf{D} = \begin{bmatrix} \mathbf{0}_{6\times6} \\ \mathbf{I}_{6\times6} \end{bmatrix}$$

for a six-axle vehicle; $\mathbf{I}$ is a unit matrix; the superscript "w/r" has the meaning of dynamic interaction between wheelsets and rail, and

$$\overline{\mathbf{P}}_i^{\mathrm{w/r}}(\omega) = \left\{ \overline{P}_{i1}^{\mathrm{w/r}}(\omega) \quad \overline{P}_{i2}^{\mathrm{w/r}}(\omega) \quad \ldots \quad \overline{P}_{iN_{\mathrm{wi}}}^{\mathrm{w/r}}(\omega) \right\}^{\mathrm{T}} \tag{7}$$

where $\overline{P}_{il}^{\mathrm{w/r}}(\omega)$ denotes the wheel–rail interaction force for the lth wheelset on the ith vehicle.

Based on Eq. (5), the vehicle vibration displacement can be expressed as

$$\overline{\mathbf{Z}}_i(\omega) = -(\mathbf{K}_i - \mathbf{M}_i\omega^2 + \mathrm{i}\mathbf{C}_i\omega)^{-1}\mathbf{D}\overline{\mathbf{P}}_i^{\mathrm{w/r}}(\omega) \tag{8}$$

Let $\overline{\mathbf{Z}}_{wi}(\omega)$ represent the wheelset displacement vector of the ith vehicle, there exists a relationship between it and the other part of the main vehicle (car-body and bogie) as

$$\overline{\mathbf{Z}}_{wi}(\omega) = \mathbf{B}\overline{\mathbf{Z}}_i(\omega) \tag{9}$$

in which the factor matrix $\mathbf{B} = [\,\mathbf{0}_{4\times6} \quad \mathbf{I}_{4\times4}\,]$ (for a four-axis vehicle) or $\mathbf{B} = [\,\mathbf{0}_{6\times6} \quad \mathbf{I}_{6\times6}\,]$ (for a six-axis vehicle).

Substituting Eq. (8) into Eq. (9) and utilizing $\mathbf{B}=\mathbf{D}^{\mathrm{T}}$, the wheelset displacement vector of the ith vehicle can be written as

$$\overline{\mathbf{Z}}_{\mathrm{w}i}(\omega)=-\mathbf{D}^{\mathrm{T}}(\mathbf{K}_i-\mathbf{M}_i\omega^2+\mathrm{i}\mathbf{C}_i\omega)^{-1}\mathbf{D}\overline{\mathbf{P}}_i^{\mathrm{w/r}}(\omega) \tag{10}$$

Eq. (10) can be further simplified as

$$\overline{\mathbf{Z}}_{\mathrm{w}i}(\omega)=-\mathbf{A}_{\mathrm{w}i}\overline{\mathbf{P}}_i^{\mathrm{w/r}}(\omega) \tag{11}$$

where $\mathbf{A}_{\mathrm{w}i}=\mathbf{D}^{\mathrm{T}}(\mathbf{K}_i-\mathbf{M}_i\omega^2+\mathrm{i}\mathbf{C}_i\omega)^{-1}\mathbf{D}$ is a complex matrix with $N_{\mathrm{w}i}\times N_{\mathrm{w}i}$ order, in which $a_{mn}^{\mathrm{w}i}$ (m=1, 2, …, $N_{\mathrm{w}i}$; n=1, 2, …, $N_{\mathrm{w}i}$) represents the displacement of the nth wheelset when a unit harmonic load with frequency ω acts on the position of the mth wheelset; $N_{\mathrm{w}i}$ is the number of wheelsets on the ith vehicle. The minus symbol "-" on the right hand side of Eq. (11) denotes that the direction of wheelset displacement is opposite to that of wheel–rail interaction force.

Assuming independent vibrations between different vehicles of a train, the following integral system vector equations can be established when Eq. (11) is applied to all wheelset displacements:

$$\overline{\mathbf{Z}}_{\mathrm{w}}=-\begin{bmatrix}\mathbf{A}_{\mathrm{w}1} & & \mathbf{0}\\ & \mathbf{A}_{\mathrm{w}2} & \\ & & \ddots \\ \mathbf{0} & & \mathbf{A}_{\mathrm{w}N_{\mathrm{v}}}\end{bmatrix}\overline{\mathbf{P}}^{\mathrm{w/r}} \tag{12}$$

where N_{v} is the number of vehicles considered in the analysis.

2.2. Track modeling

The track model composed of rails, pads, sleepers and ballast bed is simplified as a 2-level mass–spring–damper system, as shown in Fig. 1. The rail is considered as an infinite Euler–Bernoulli beam on elastic supports (pads and fasteners), and the sleeper as a mass with only vertical movement. The spring–damper system between the rail and the sleepers is represented by k_{rs} and c_{rs}, and that between the sleepers and roadbed represented by k_{sg} and c_{sg}, respectively.

When a train runs on the track with speed V, the wavelength and the circular frequency of track irregularity can be expressed with respect to spatial angular frequency Ω as $\lambda=2\pi/\Omega$ and $\omega=\Omega V=2\pi V/\lambda$, respectively. The sample function of track irregularity series can be regarded as the superposition of a series of harmonic components with different frequencies and phases. When considering a single spatial angular frequency only, the track irregularity can be expressed as

$$z_{\mathrm{r}}^{k}(x)=\tilde{z}_{\mathrm{r}}(\Omega_k)\mathrm{e}^{\mathrm{i}\Omega_k x} \tag{13}$$

In actual analysis, the track irregularity at position $x_{\mathrm{p}il}=x_{\mathrm{p}il}^0+Vt$ can also be described as the function of time t that a moving wheel travels from its initial position:

$$z_{\mathrm{r}il}^{k}(t)=\overline{z}_{\mathrm{r}il}(\omega_k)\mathrm{e}^{\mathrm{i}\omega_k t} \tag{14}$$

where $x_{\mathrm{p}il}^0$ is the initial position coordinate of the lth wheelset of the ith vehicle. The amplitude of track irregularity corresponding to frequency ω_k can then be written as

$$\overline{z}_{\mathrm{r}il}(\omega_k)=\tilde{z}_{\mathrm{r}}(\Omega_k)\mathrm{e}^{\mathrm{i}(\omega_k/V)x_{\mathrm{p}il}^0} \tag{15}$$

For the whole train, the track irregularities corresponding to all wheelset positions can be expressed as the following vector:

$$\begin{Bmatrix}\overline{\mathbf{z}}_{\mathrm{r}1}(\omega_k)\\ \overline{\mathbf{z}}_{\mathrm{r}2}(\omega_k)\\ \vdots\\ \overline{\mathbf{z}}_{\mathrm{r}N_{\mathrm{v}}}(\omega_k)\end{Bmatrix}=\tilde{z}_{\mathrm{r}}(\Omega_k)\cdot\begin{Bmatrix}\mathbf{e}_1(\omega_k)\\ \mathbf{e}_2(\omega_k)\\ \vdots\\ \mathbf{e}_{N_{\mathrm{v}}}(\omega_k)\end{Bmatrix} \tag{16}$$

where

$$\mathbf{e}_i(\omega_k)=\left\{\mathrm{e}^{\mathrm{i}(\omega_k/V)x_{\mathrm{p}i1}^0}\quad \mathrm{e}^{\mathrm{i}(\omega_k/V)x_{\mathrm{p}i2}^0}\quad \dots\quad \mathrm{e}^{\mathrm{i}(\omega_k/V)x_{\mathrm{p}iN_{\mathrm{w}i}}^0}\right\}^{\mathrm{T}} \tag{17}$$

$$\overline{\mathbf{z}}_{\mathrm{r}i}(\omega_k)=\left\{\overline{z}_{\mathrm{r}i1}(\omega_k)\quad \overline{z}_{\mathrm{r}i2}(\omega_k)\quad \dots\quad \overline{z}_{\mathrm{r}iN_{\mathrm{w}i}}(\omega_k)\right\}^{\mathrm{T}} \tag{18}$$

2.3. Subsoil modeling

It is well known that the dynamic properties of soil material can be divided into three kinds of working states on the basis of the dynamic strain ε of the soil: (1) elastic state when $\varepsilon<10^{-4}$; (2) elastic–plastic state when $\varepsilon=10^{-4}$–10^{-2}; (3) plastic state when $\varepsilon>10^{-2}$. As the dynamic strain of ground soil induced by rail traffic is generally 10^{-5} or much smaller, the soil model in this study is assumed to be elastic. The good vibration prediction for the ground alongside the track requires a reasonable subsoil model. The generation of eigenwaves and their propagation are uniquely characterized by the

constituting layer properties of the ground. Herein, the subsoil under the track is modeled as a three-dimensional layered viscoelastic medium with the bottom modeled as half-space (shown in Fig. 2), by assumming each of the parallel layers isotropic and homogeneous. The wave propagation in the soil is characterized by the dynamic Green's function of ground displacement, which can be found in the authors' previous work [20,21].

2.4. Coupling analysis between submodels

The interaction forces between the vehicle and the track and between the track and the subsoil are illustrated in Fig. 3.

2.4.1. Coupling of vehicle and track

The coupling of vehicle and track is accomplished by the wheel–rail contact relationship assumed by the Hertz contact theory. The wheel–rail interaction force for the lth wheelset of the ith vehicle can be expressed as follows:

$$P_{il}^{w/r}(t) = k_H[z_{wil}(t) - w_{ril}(t) - z_{ril}(t)] \tag{19}$$

where k_H is the wheel–rail contact stiffness; $z_{wil}(t)$ the wheelset displacement; $w_{ril}(t)$ the vertical rail displacement induced by moving load $P_{il}^{w/r}(t)$; $z_{ril}(t)$ the variation profile of track irregularity, and that $P_{il}^{w/r}(t)$ is equal toP_{i0} in the case of quasi-static state with $z_{ril}(t) = 0$.

Using the Fourier transform, Eq. (19) can be expressed as

$$\overline{P}_{il}^{w/r}(\omega_k) = k_H[\overline{z}_{wil}(\omega_k) - \overline{w}_{ril}(\omega_k) - \overline{z}_{ril}(\omega_k)] \tag{20}$$

A set of vector equations in the frequency domain for all wheel–rail contact forces can be obtained when Eq. (20) is applied to all wheel–rail contact points:

$$\overline{\mathbf{P}}^{w/r} = k_H \cdot (\overline{\mathbf{Z}}_w - \overline{\mathbf{W}}_r - \overline{\mathbf{Z}}_r) \tag{21}$$

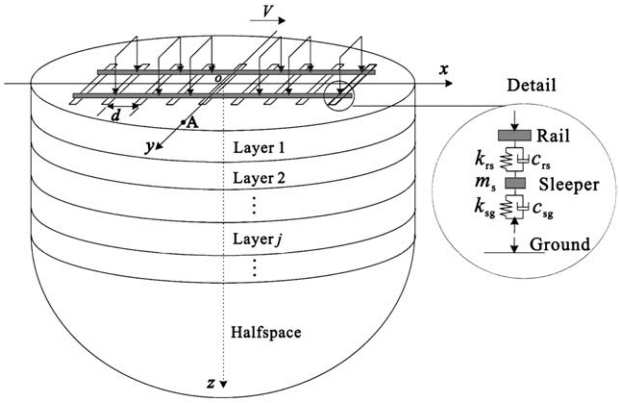

Fig. 2. Track–soil dynamic interaction model.

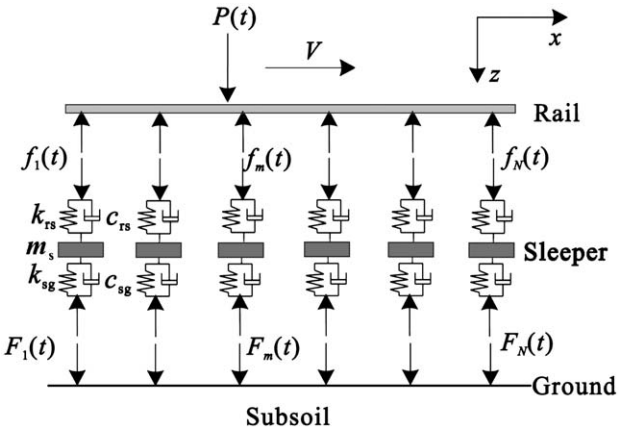

Fig. 3. Illustration of interaction forces among train, track and soil.

in which $\overline{\mathbf{Z}}_w$ is the wheelset displacement vector; $\overline{\mathbf{Z}}_r$ the track irregularity profile vector; $\overline{\mathbf{W}}_r$ the rail displacement vector expressed as

$$\overline{\mathbf{W}}_r = \overline{\mathbf{G}}^1_{rail}(\overline{\mathbf{P}}_0 + \overline{\mathbf{P}}^{w/r}) - \overline{\mathbf{G}}^2_{rail}\overline{\mathbf{f}} \tag{22}$$

where $\overline{\mathbf{P}}_0$ is the quasi-static excitation vector induced by moving gravity axle loads; $\overline{\mathbf{G}}^1_{rail}$ and $\overline{\mathbf{G}}^2_{rail}$ are transfer matrices with different dimensions constituted by the Green's functions of rail displacements at the positions of $2N+1$ sleepers, which can be referenced in the author's previous works [20]; $\overline{\mathbf{f}} = \{\overline{f}_{-N}(\omega), \ldots, \overline{f}_0(\omega), \ldots, \overline{f}_N(\omega)\}^T$ is a column vector made up of support reactions on the rail from $2N+1$ sleepers, and N is the number of sleepers that develop effective influence on the ground vibration.

2.4.2. Coupling of track and soil

In the frequency domain, the dynamic equilibrium equations of the $2N+1$ sleepers can be written as

$$\overline{\mathbf{f}} - \overline{\mathbf{F}} = m_s\omega^2\overline{\mathbf{W}}_s \tag{23}$$

and

$$\overline{\mathbf{f}} = (k_{rs} + i\omega c_{rs})(\overline{\mathbf{W}}_s - \overline{\mathbf{W}}_r) \tag{24}$$

where $\overline{\mathbf{F}} = \{\overline{F}_{-N}(\omega), \ldots, \overline{F}_0(\omega), \ldots, \overline{F}_N(\omega)\}^T$ is the column vector consisting of $2N+1$ sleeper–soil interaction forces; $\overline{\mathbf{W}}_s = \{\overline{w}_s(x_{-N}, \omega), \ldots, \overline{w}_s(x_0, \omega), \ldots, \overline{w}_s(x_N, \omega)\}^T$ the column vector consisting of $2N+1$ sleeper displacements.

The track model and the soil model are connected with sleepers, and the interaction forces between sleepers and ground surface are as follows:

$$\overline{\mathbf{F}} = (k_{sg} + i\omega c_{sg})(\overline{\mathbf{U}}_z - \overline{\mathbf{W}}_s) \tag{25}$$

where $\overline{\mathbf{U}}_z = \{\overline{u}_z(x_{-N}, \omega), \ldots, \overline{u}_z(x_0, \omega), \ldots, \overline{u}_z(x_N, \omega)\}^T$ is a column vector consisting of $2N+1$ ground displacements at the position of sleepers.

On the other hand, for a layered-soil bottomed of a half-space, the $2N+1$ ground displacements at the position of sleepers can be expressed in a vector equation:

$$\overline{\mathbf{U}}_z = \overline{\mathbf{G}}_{zz}\overline{\mathbf{F}} \tag{26}$$

where $\overline{\mathbf{G}}_{zz}$ is the $(2N+1)\times(2N+1)$ order matrix that consists of the Green's functions of ground displacements, which can be found in the authors' previous work [20,21].

2.5. Ground displacement

When the soil reaction vector $\overline{\mathbf{F}}$ under moving train loads is obtained by solving the simultaneous equations combined by Eqs. (12), (16) and (21)–(26), the total ground displacement at the concerned location A can be acquired by the superposition of all the displacement components induced by each of the subsoil reactions under the $2N+1$ sleepers. The solution expression is as follows:

$$\overline{u}_{zz}(y, 0, \omega) = \overline{\mathbf{F}} \cdot \overline{\mathbf{G}}^*_{zz} \tag{27}$$

where $\overline{\mathbf{G}}^*_{zz}$ is the vector consisting of the Green's functions of ground displacements at the location of A induced by $2N+1$ subsoil reactions:

$$\overline{\mathbf{G}}^*_{zz} = \{\overline{G}_{zz}(r_{-N}, 0, \omega), \ldots, \overline{G}_{zz}(r_0, 0, \omega), \ldots, \overline{G}_{zz}(r_N, 0, \omega)\} \tag{28}$$

where $r_m = \sqrt{(md)^2 + y^2}$ is the distance between the mth sleeper and the observation point A, y the distance of A from the track, and d the sleeper spacing (Ref. Fig. 4).

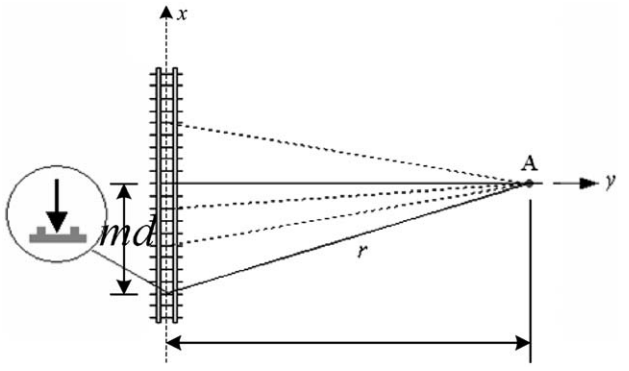

Fig. 4. Influence of different subsoil reactions on the ground displacement at Location A.

A computer code for solving the train–track–soil interaction model is developed via MATLAB based on the formulations described above and is employed to perform a case study.

3. Case study

3.1. Calculation parameters

The *China-star* train composed of 1 locomotive plus 4 passenger cars plus 1 locomotive is taken as the train load, and detailed parameters of the vehicles can be found in [22].

The track parameters include:

Rail: mass per unit length $\overline{m}_r$=60 kg/m, section stiffness EI=6.63 × 10^6 N m^2, damping ratio ξ_r=0.01.

Sleeper: mass m_s=250 kg; spacing d=0.55 m.

Ballast bed: mass participating in vibration m_b=560 kg; Spring–damper coefficients k_{rs}=7.8 × 10^7 N/m, c_{rs}=5.0 × 10^4 N s/m, k_{sg}=6.5 × 10^7 N/m and c_{sg}=9.0 × 10^4 N s/m.

The track irregularity is simulated by a single wavelength harmonic profile with the irregularity amplitude $\tilde{z}_r(\Omega_k)$ equal to 0.2 mm in Eq. (16).

The soil parameters listed in Table 1 are taken from the geological survey on the alluvial plain of the Yellow River [23]. The ground water level is −3 m below the ground surface. In order to describe the subsoil properties more clearly, the dispersion diagram for the ground structure (without track) is shown in Fig. 5, i.e., the wavenumbers of propagating modes in the ground are plotted against frequency. In this Figure, the modes involving coupled compression and vertically polarized shear wave motion (P-SV modes) are marked with solid lines. Since the modes involving horizontally polarized shear motion (SH modes) have no component of vertical motion and in this paper only the vertical train–track dynamics are considered, the SH modes are not excited in the model and not illustrated herein. The lower dashed line is the dispersion curve of the bottom half-space soil, which corresponds exactly to the shear wave velocity of the bottom half-space soil; while the upper dashed line just corresponds to the Rayleigh's wave velocity of the top layer soil.

From the dispersion diagram it can be seen that at high frequency, the wavenumber of the first P-SV mode converges towards that of a Rayleigh's wave of the top layer material; in addition at about 24.57 Hz the second P-SV mode arises, the third appears just above 43.99 Hz and the fourth about 81.78 Hz. These intersection frequencies where the amount of

Table 1
Parameters of layered half-space soil.

Layer	Soil type	Depth (m)	Density (kg/m^3)	Elastic modulus (MPa)	Cohesive force (kPa)	Internal frictional angle (deg)	Poisson ratio	Damping ratio	Wave velocity (m/s)		
									C_P	C_S	C_R
1	Loessal mild clay	3.0	1350	95.59	15	18	0.37	0.05	350	161	151
Half-space	Loessal silty clay	–	1898	506.97	30	19	0.48	0.05	1700	300	285

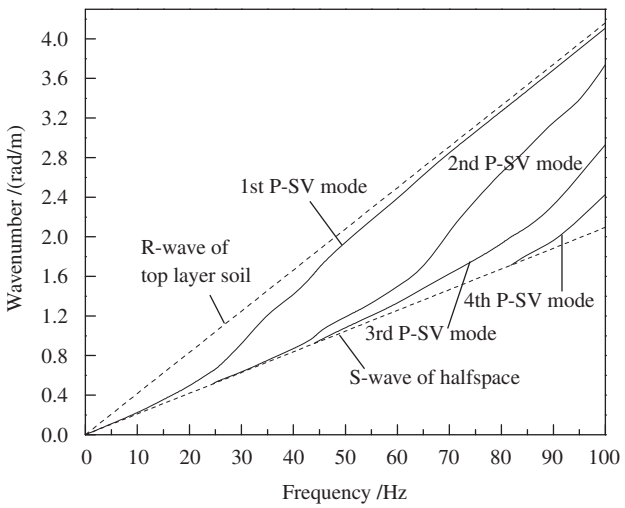

Fig. 5. Dispersion diagram for the P-SV modes in the ground soil.

modes will change are so-called cut-off frequencies of layer soil. In fact, different ground soil structures have different cut-off frequencies that may be called natural frequencies of layered half-space soil model.

3.2. Vibration analysis of track structure and ground surface

Plotted in Fig. 6 are the vertical acceleration histories of rail, sleeper, and observation point A at 0, 5, 20 and 30 m from the track on the ground surface, under the train speed of 200 km/h.

The attenuation and propagation of vibration in the track–soil system can be observed from the figure as follows:

(1) The acceleration amplitudes of the track–soil system decrease successively from rail to sleeper and from sleeper to ground soil: the maximum acceleration of rail is up to 120 m/s^2, and it decreases to about 25 m/s^2 for sleeper and 1.2 m/s^2 for ground surface under sleeper.
(2) The ground acceleration attenuates with the distance increase to the track, and with the increase of distance, the relevance of ground acceleration curves and the train excitation becomes less and less obvious. This observation is in accordance with the experimental results in [24,25].

The acceleration spectra for observation point A at y=0, 5 and 20 m on the ground surface are shown in Fig. 7. It can be found that with the increase of distance to the track, the higher frequency components of acceleration spectra become lesser and lesser, which can be explained by the dissipation of material damping and radiation damping in soil medium to higher frequency components in vibration energy.

3.3. Influence of speed of moving loads and soil property on ground vibration

The forces applied to the track structure by a moving train mainly consist of two components: the quasi-static excitation induced by moving gravity axle-loads and the wheel–rail dynamic excitation induced by irregularity of wheel–rail contact surface. In this section, the moving unit-constant-load and the moving unit-harmonic-load are adopted to analyze the influence of train speed and soil property on ground vibrations, respectively, in the cases of quasi-static excitation and dynamic excitation.

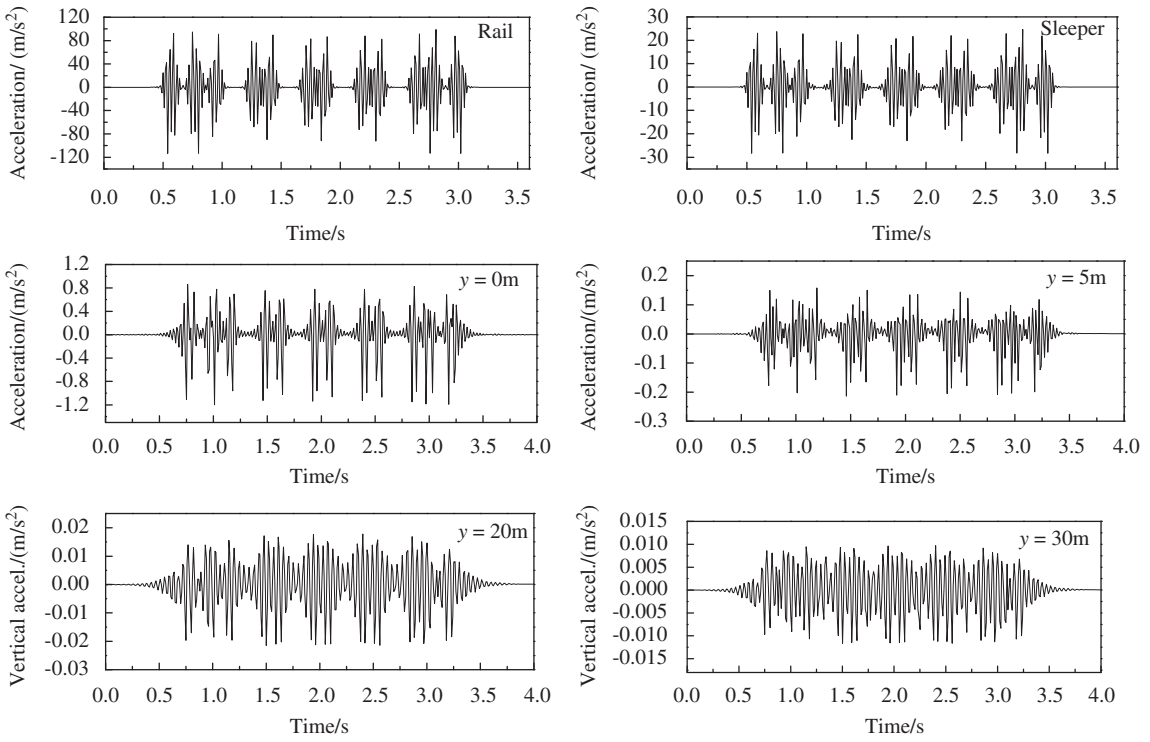

Fig. 6. Acceleration histories of rail, sleeper, and different observation points on the ground.

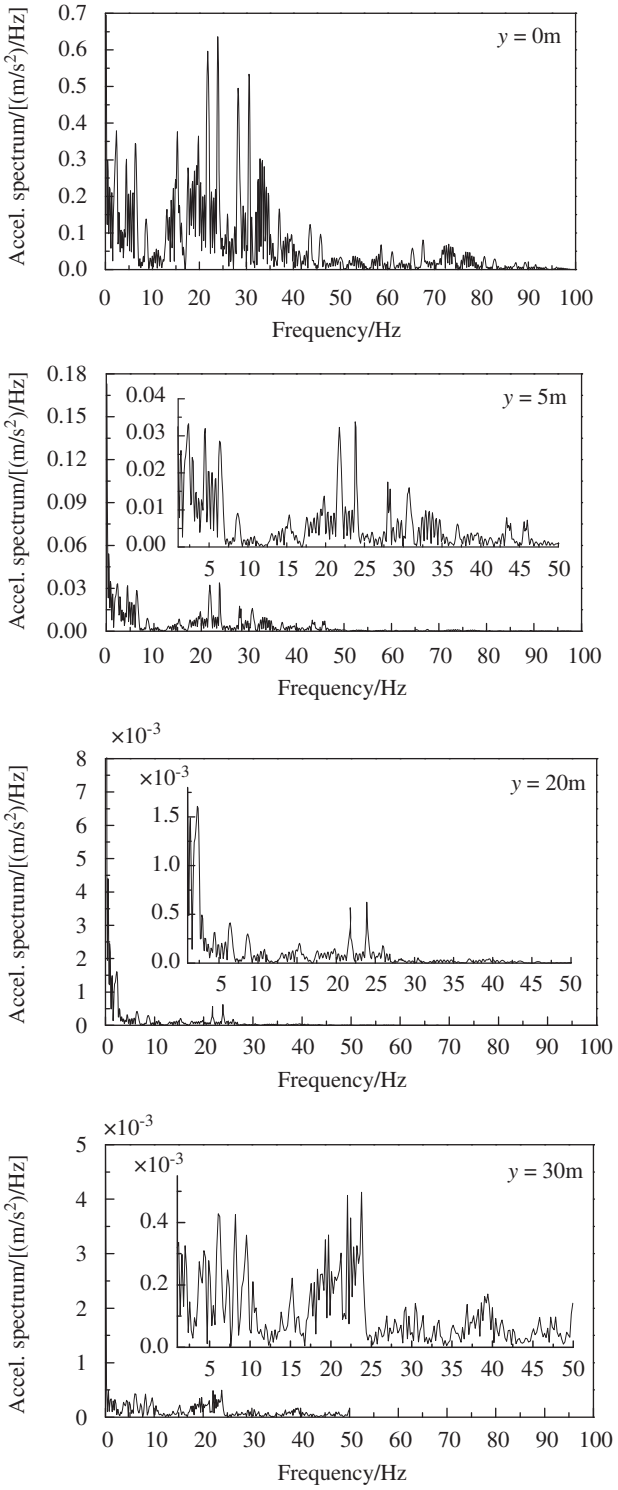

Fig. 7. Acceleration spectra of different observation points on the ground.

3.3.1. Ground vibration induced by moving unit-constant-load

The vertical ground displacements induced by moving unit-constant-loads with the speed of 100, 151, 200, 250 and 280 m/s are calculated by using the above train–track–soil dynamic interaction model, and the displacement spectra of two observation points (y=0 and 8 m) are respectively plotted in Figs. 8 and 9.

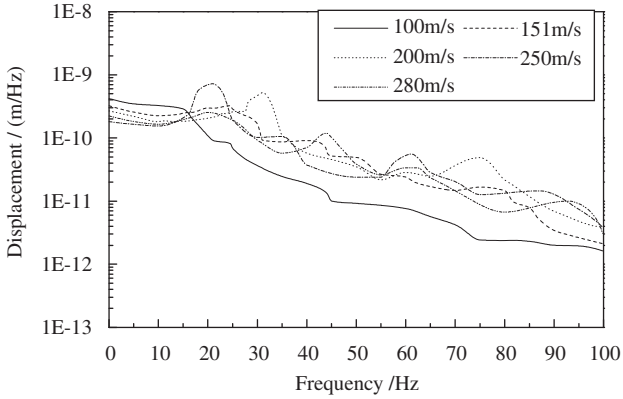

Fig. 8. Spectra of ground displacement induced by moving constant-load (y=0 m).

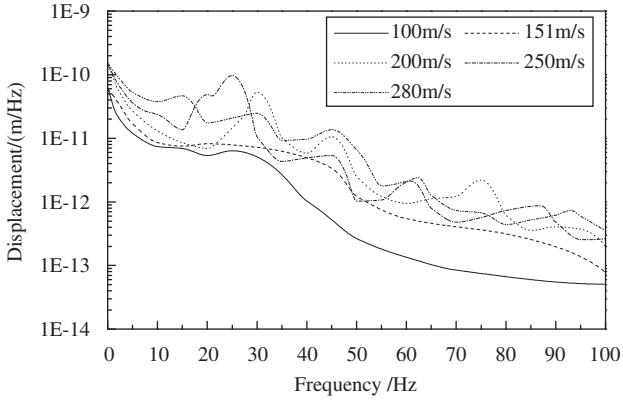

Fig. 9. Spectra of ground displacement induced by moving constant-load (y=8 m).

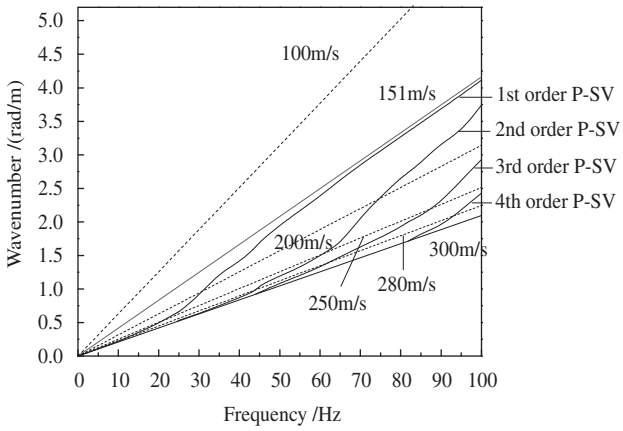

Fig. 10. Distribution of P-SV dispersion curves and constant-load speed-lines.

It can be observed from the figures that there exist amplification phenomena of ground vibration corresponding to different frequencies for different moving speeds, which may be explained hereafter as due to the soil resonance induced by loads moving at certain speeds. According to soil dynamics and structure dynamics, the resonance frequencies of layered-soil corresponding to the moving loads are the intersection frequencies of the moving load speed-lines and the subsoil dispersion curves. Plotting the first four orders of P-SV dispersion curves of the layered-soil and the five speed-lines of moving constant-loads that are graphed on the basis of $k = 2\pi f/V$ in a same coordinate system (Fig. 10), one can find their intersection frequencies, i.e. resonance frequencies of the layered-soil. Detailed values of them are listed in Table 2.

The following characteristics can be summarized from the intersection frequencies observed in Fig. 10 and Table 2, and by comparing those with the curves in Figs. 8 and 9:

(1) When the moving speed of constant-load is not higher than the Rayleigh's wave speed of the top layer soil (151 m/s), the displacement spectra emerge a monotonous descending tendency. In this case, there are no intersections of speed-lines and dispersion curves appeared, which shows that the ground vibration frequencies excited by the moving loads cannot reach the resonance frequencies of the soil. This phenomenon indicates that when the speed of moving load is much smaller than the Rayleigh's wave speed, the soil vibration induced by the moving load is close to that induced by a static load.
(2) When the moving speed of constant-load is higher than the Rayleigh's wave speed of the top layer soil, one or more vibration peaks may appear. In this case, there exist several intersections for the speed-lines and the dispersion curves, the number of which is related to the speed of moving loads, and the frequencies corresponding to the vibration peaks are close to the resonance frequencies of the soil.
(3) When the resonance frequencies of the soil corresponding to the speed of moving loads are close to the natural frequencies (i.e. the cut-off frequencies) of the layered-soil, the ground vibration is amplified. This explains why the maximal displacement peaks shown in Figs. 8 and 9 occur under the moving load speed of 250 m/s: the resonance frequency corresponding to this load-speed is 21 Hz and it is close to the first-order cut-off frequency 24.57 Hz of the soil.

3.3.2. *Ground vibration induced by moving unit-harmonic-load*

Since the first-order and the second-order cut-off frequencies of the subsoil are respectively 24.57 and 43.99 Hz, the vibration frequency 35 Hz in this range for the unit-harmonic-load is selected, to well observe the intersection frequencies. The speed-lines of moving harmonic-loads and the P-SV dispersion curves of the subsoil model are plotted in Fig. 11, and the corresponding intersection frequencies are listed in Table 3. In this case, the speed-lines of moving harmonic-loads are determined by $k = 2\pi|f - f_0|/V$, thus one can find two groups of speed-lines starting from the loading frequency f_0=35 Hz.

The vertical ground displacements induced by the moving unit-harmonic-loads with the speed of 100, 151, 200 and 250 m/s are calculated, and the displacement spectra of two observation points (y=0 and 8 m) are illustrated in Figs. 12 and 13, respectively.

It can be found that the frequencies corresponding to displacement peaks in Figs. 12 and 13 are close to the intersection frequencies listed in Table 3, which shows that in the case of moving harmonic loads, the appearance of ground vibration amplification is also at the resonance frequency of the soil and the moving loads.

Table 2
Intersection frequencies of constant-load speed-lines and P-SV dispersion curves (Hz).

Modes of layer soil	Speeds of moving load V (m/s)				
	100	151	200	250	280
First-order	–	–	31	21	–
Second-order	–	–	75	61	44
Third-order	–	–	–	87	62.3
Fourth-order	–	–	–	–	93

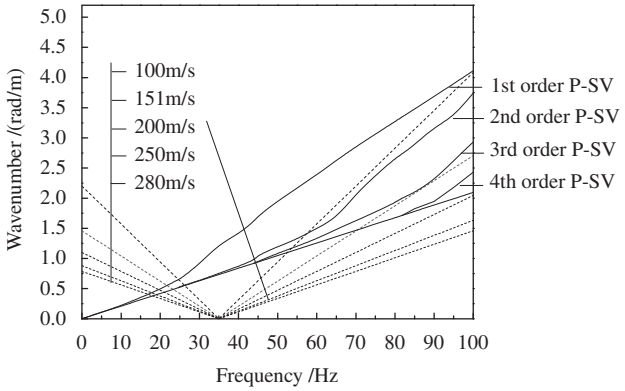

Fig. 11. Distribution of P-SV dispersion curves and harmonic-load speed-lines.

Table 3
Intersection frequencies of P-SV dispersion curves and harmonic-load speed-lines (Hz).

Modes of layer soil	Speeds of moving load V (m/s)				
	100	151	200	250	280
First-order	24.67 101	21.72	19.59	17.89	16.91
Second-order	26 57.4	–	–	–	–
Third-order	53.83	–	–	–	–
Fourth-order	–	–	–	–	–

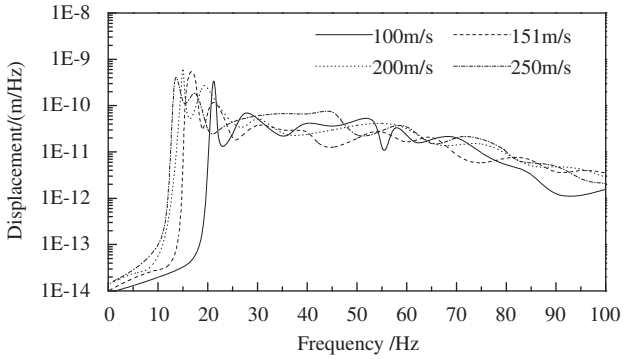

Fig. 12. Spectra of ground displacement induced by moving harmonic-load (y=0 m).

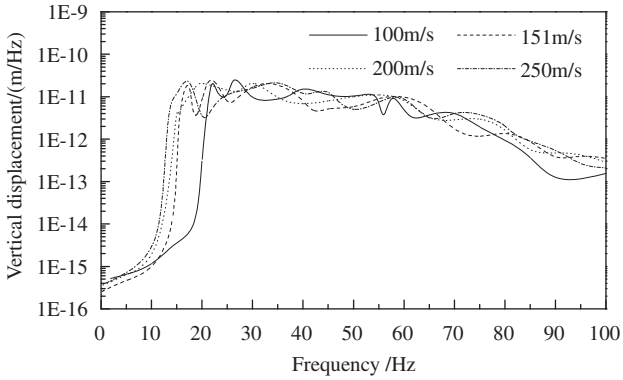

Fig. 13. Spectra of ground displacement induced by moving harmonic-load (y=8 m).

As can be seen from Figs. 12 and 13, the displacement spectra of ground vibrations induced by moving harmonic-loads are mostly at the same order of magnitude, in which the higher frequency components are more abundant than those in the case of moving constant-loads, and the influence of their moving speed on ground vibration is smaller than that by constant-loads. The frequencies of ground vibration induced by harmonic-loads are within a certain range, and the higher the moving speed, the wider the frequency range. These observations are in accordance with the results in Ref. [26] that the frequency of ground vibration induced by moving harmonic-loads mainly concentrates on the range of $[\omega_0/(1+V/C), \omega_0/(1-V/C)]$, in which ω_0 is the vibration frequency of harmonic-load (35 Hz herein), V is the moving speed, and C is the Rayleigh's wave speed of top-layer soil model (151 m/s herein).

4. Conclusions

Based on the vehicle dynamics, track dynamics and the Green's functions of subsoil obtained in the authors' previous works [20,21], a train–track–soil dynamic interaction model is established in this paper. The models take account of the

vibrations of vehicle components, the quasi-static axle loads and the dynamic excitations between the wheels and track, with track irregularity simulated by a single wavelength harmonic profile. The train submodel, the track submodel and the subsoil submodel are coupled through dynamic interactions of wheel–rail and sleeper-soil, respectively. A computer code for solving the train–track–soil interaction model is developed via MATLAB and is employed to perform a case study, through which the moving train induced vibrations of the rail, the sleeper, and the ground surface are worked out. The main results include:

(1) When the moving constant-load speed is much lower than the Rayleigh's wave speed of the subsoil, the corresponding soil vibration is similar to that induced by static loads.
(2) Whether under the quasi-static excitation or the wheel–track dynamic excitation, the characteristics of ground vibrations have a close relationship with train speed and soil properties.
(3) The dynamic excitation produced by wheel–track irregularity has big influence on the higher frequency components of ground vibration; therefore, it is unreasonable to consider only the quasi-static loads in the source model.
(4) With the increase of distance to the track, the ground acceleration has the tendency of decrease, and the relevance of acceleration curves and train excitation becomes less obvious.
(5) The intersection frequencies of the speed-lines of moving train and the dispersion curves of subsoil are some resonance frequencies that cause the amplification of ground vibrations.
(6) There exists a critical speed for moving train that is close to the minimum speed of the Rayleigh's wave in the subsoil.

Acknowledgments

This research is supported by the Key Project of the Natural Science Foundation of China (Grant no. 50538010), the Natural Science Foundation of Beijing (Grant no. 8082021), and the Flander (Belgium)–China Bilateral Project (Grant no. BIL 07/07).

References

[1] V.V. Krylov, C. Ferguson, Calculation of low-frequency ground vibrations from railway trains, *Applied Acoustics* 42 (1994) 199–213.
[2] V.V. Krylov, Generation of ground vibration by superfast trains, *Applied Acoustics* 44 (1995) 149–164.
[3] V.V. Krylov, Effects of track properties on ground vibrations generated by high-speed trains, *ACUSTICA acta acustica* 84 (1998) 78–90.
[4] G. Lombaert, G. Degrande, Ground-borne vibration due to static and dynamic axle loads of InterCity and high-speed trains, *Journal of Sound and Vibration* 319 (3–5) (2009) 1036–1066.
[5] C.J.C. Jones, J.R. Block, Prediction of ground vibration from freight trains, *Journal of Sound and Vibration* 193 (1) (1996) 205–213.
[6] A. Karlström, A. Boström, An analytical model for train-induced ground vibrations from railways, *Journal of Sound and Vibration* 292 (2006) 221–241.
[7] X. Sheng, C.J.C. Jones, et al., Ground vibration generated by a load moving along a railway track, *Journal of Sound and Vibration* 228 (1) (1999) 129–156.
[8] X. Sheng, C.J.C. Jones, et al., A theoretical model for ground vibration from trains generated by vertical track irregularities, *Journal of Sound and Vibration* 272 (2004) 937–965.
[9] C. Madshus, A.M. Kaynia, High-speed railway lines on soft ground: dynamic behavior at critical train speed, *Journal of Sound and Vibration* 231 (3) (2000) 689–701.
[10] A.M. Kaynia, C. Madshus, L. Harvik, et al., Ground vibration from high-speed trains: prediction and countermeasure, *Journal of Geotechnical and Geoenvironmental Engineering, American Society of Civil Engineers* 120 (6) (2000) 531–537.
[11] H. Takemiya, Ground vibrations alongside tracks induced by high-speed trains: prediction and mitigation, in: V.V. Krylov (Ed.), *Noise and Vibration from High-speed Trains*, Thomas Telford, London, 2001, pp. 347–393.
[12] H. Takemiya, Simulation of track–ground vibrations due to a high-speed train: the case of X-2000 at Ledsgard, *Journal of Sound and Vibration* 261 (2003) 503–526.
[13] Y.B. Yang, H.H. Hung, A 2.5 D finite/infinite element approach for modeling visco-elastic bodies subjected to moving loads, *International Journal for Numerical Methods in Engineering* 51 (11) (2001) 1317–1336.
[14] Y.B. Yang, Train-induced wave propagation in layered soils using finite/infinite element simulation, *Soil Dynamics and Earthquake Engineering* 23 (2003) 263–278.
[15] M. Katou, T. Matsuoka, O. Yoshioka, et al., Numerical simulation study of ground vibrations using forces from wheels of a running high-speed train, *Journal of Sound and Vibration* 318 (2008) 830–849.
[16] L. Auersch, The excitation of ground vibration by rail traffic: theory of vehicle–track–soil interaction and measurements of high-speed lines, *Journal of Sound and Vibration* 284 (2005) 103–132.
[17] X. Sheng, C.J.C. Jones, D.J. Thompson, Prediction of ground vibration from trains using the wavenumber finite and boundary element methods, *Journal of Sound and Vibration* 293 (2006) 575–586.
[18] P. Galvín, J. Domínguez, Analysis of ground motion due to moving surface loads induced by high-speed trains, *Engineering Analysis with Boundary Elements* 31 (2007) 931–941.
[19] P. Galvín, J. Domínguez, High speed train-induced ground motion and interaction with structures, *Journal of Sound and Vibration* 307 (2007) 755–777.
[20] Y.M. Cao, Theoretical and Experimental Study on Train-induced Vibrations of Free Field and Buildings, Doctoral Thesis, Beijing Jiaotong University, Beijing, 2006.
[21] Y.M. Cao, H. Xia, Analysis of Green's functions in wavenumber–frequency domain for surface displacements of elastic layered half-space soil, *Journal of Computer Mechanics* 25 (6) (2008) 283–288.
[22] H. Xia, N. Zhang, Dynamic analysis of railway bridge under high-speed trains, *Computers and Structures* 83 (2005) 1891–1901.
[23] The Soil Dynamics Committee of Vibration Engineering Association of China, *Application Analysis of Soil Dynamics in Engineering*, China Architecture and Building Press, Beijing, 1998, pp. 44–46 (in Chinese).
[24] H. Xia, N. Zhang, Y.M. Cao, Experimental study of train-induced vibrations of environments and buildings, *Journal of Sound and Vibration* (280) (2005) 1017–1029.
[25] J.G. Chen, H. Xia, et al., Experimental study of ground vibrations induced by moving train, *Journal of Rock and Soil Mechanics* 29 (11) (2008) 3113–3118 (in Chinese).
[26] G. Lombaert, *Development and Experimental Validation of a Numerical Model for the Free Vibrations Induced by Road Traffic*, Leuven University, Belgium, 2001.